Element distributions after binary fission of ^{44}Ti

R. Płaneta,[a] P. Belery,[b] J. Brzychczyk,[a] P. Cohilis,[b] Y. El Masri,[b] Gh. Grégoire,[b] K. Grotowski,[c]* Z. Majka,[a] S. Micek,[a] M. Szczodrak,[a] A. Wieloch,[a] and J. Albiński[a]

[a] *Institute of Physics, Jagellonian University, Institute of Nuclear Physics, Kraków, Poland*

[b] *Institute of Nuclear Physics, Université Catholique de Louvain, B-1348 Louvain-la-Neuve, Belgium*

[c] *Kernforschungszentrum Karlsruhe, Institut für Kernphysik, Karlsruhe, Federal Republic of Germany*

(Received 14 February 1986)

Inclusive and coincidence measurements have been performed to study symmetric fragmentation of ^{44}Ti binary decay from the $^{32}S+^{12}C$ reaction at 280 MeV incident energy. Element distributions after binary decay were measured. Angular distributions and fragment correlations are presented. Total c.m. kinetic energy for the symmetric products is extracted from our data and from Monte-Carlo model calculations including Q-value fluctuations. This result was compared to liquid drop model calculations and standard fission systematics. Comparison between the experimental value of the total kinetic energy and the rotating liquid-drop model predictions locates the angular momentum window for symmetric splitting of ^{44}Ti between $33\hbar$ and $38\hbar$. It also showed that 50% of the corresponding rotational energy contributes to the total kinetic energy values. The dominant reaction mechanism was found to be symmetric splitting followed by evaporation.

I. INTRODUCTION

Recently, the existence of symmetric or nearly symmetric decay of three light systems, $^{12}C+^{40}Ca\rightarrow^{52}Fe^*$, $^{9}Be+^{40}Ca\rightarrow^{49}Cr^*$, and $^{6}Li+^{40}Ca\rightarrow^{46}V^*$, has been established in a coincidence experiment.[1]

In the range of center-of-mass (c.m.) angles 45°–115° the data suggest an angular distribution $\sim 1/\sin\theta_{\text{c.m.}}$, which is expected from the decay of a system with a lifetime at least equal to or greater than a rotation period.[2] Also, the excitation function for symmetric products from $^{12}C+^{40}Ca$ is indicative of a fusion-fission–like process.

Total c.m. kinetic energies measured[1] together with the rotating liquid drop model (RLDM) calculations[3,4] indicate that the window for symmetric decay is located at high angular momenta ($l\simeq 30\hbar$). As predicted by the RLDM,[5] the nuclei in question ($A\simeq 50$) are, for $l\simeq 30\hbar$, strongly deformed. Even they are slightly triaxial (the Beringer-Knox shape), with the ratio $R_{\max}/R_{\min}\geq 2$, compatible with superdeformed nuclei. Recent calculations[6] showed that at $A=56$ the inclusion of shell model corrections results in an even more elongated configuration, $R_{\max}/R_{\min}\simeq 3$.

In the present experiment we studied the fission channel for the 280 MeV $^{32}S+^{12}C\rightarrow^{44}Ti^*$ reaction. Due to reversed kinematics, fragment energies are high (no energy threshold limitations) and measurements could cover a wide range of c.m. angles, 30°–170°.

At 280 MeV incident energy the primary decay fragments from ^{44}Ti are excited up to about 20 MeV, and lose a significant fraction of mass, and charge ($\simeq$10%), by sequential particle emission. Therefore, the resulting recoil changes in the primary velocity and direction induce broadening in the measured energy distributions and correlation curves. Another important effect is the fluctuation of the Q value at the scission point.

In this work both recoil and Q value fluctuation effects are treated in a systematic way. Consequently, it was possible to obtain information on relative probabilities of symmetric decay of the ^{44}Ti nucleus characterized by fragment to charge ratio 11:11, and its asymmetric decay defined by the ratios 10:12 and 9:13. We were also able to select the incomplete fusion-fission channel.

The most probable c.m. total kinetic energy (TKE) of decay fragments measured in this work provides a new value for the Viola fission systematics.[7,8]

In Sec. II of this paper experimental details are given. Problems related to light particle evaporation and the resulting missing charge ΔZ observed in the coincidence measurements are discussed in Sec. III. Angular correlation data, presented and discussed in Sec. IV, are confronted with a Monte Carlo simulation model. Angular distributions of decay fragments are shown in Sec. V. Properties and fission of the compound system $^{32}S+^{12}C\rightarrow^{44}Ti^*$ are studied in Sec. VI in terms of the RLDM. The summary and a discussion are given in Sec. VII.

II. EXPERIMENTAL SETUP AND PROCEDURE

A beam of $^{32}S^{9+}$ ions delivered by an ECR (electron cyclotron resonance) source, was accelerated up to 280 MeV in the variable energy cyclotron CYCLONE of the University of Louvain and focused on a carbon target 0.76 mg/cm^2 thick. The reaction products were detected by two ΔE-E gas-silicon telescopes positioned on rotatable arms inside a 100 cm diam scattering chamber. The beam intensity (up tp 200 nA) was limited by the counting rates of the gas detectors. The rectangular (5×10 mm^2) entrance windows of the telescopes subtended solid angles of $\sim$1.4 msr and determined an angular resolution of $\pm 0.8°$. Solid angles were measured using a source of known activity. The energy scale of the telescopes was calibrated at low energy with an ^{241}Am source and at high energy by a

 ©1986 The American Physical Society

$^{12}C^{3+}$, $^{16}O^{4+}$, and $^{32}S^{8+}$ mixed beam of ions with respective energies 83.0, 106.0, and 221.1 MeV, elastically scattered by a gold target.

The beam charge was collected in a Faraday cup equipped with an electrostatic suppressor of secondary electrons and connected to a standard current digitizer. The correction for effective charge of the sulfur beam after passing the carbon target was taken into account.[9]

The E, ΔE, and time correlation signal between the telescopes (TAC) were registered on magnetic tapes in an event by event mode. In measurements where singles and coincidence events were recorded simultaneously, the singles data were scaled down by an appropriate factor to keep computer dead time sufficiently low. The random coincidence events were always less than 1% of the real ones.

A typical E vs ΔE map for products from the reaction 280 MeV $^{32}S+^{12}C$ is shown in Fig. 1. Ridges correspond to nuclei with atomic numbers ranging from $Z=5$ up to $Z=16$. Absolute Z calibration was provided by the elastic scattering groups of ^{12}C, ^{16}O, and ^{32}S ions. The elastic scattering group of ^{32}S ions is clearly visible in the upper right part of Fig. 1. The errors introduced in the Z separation procedure was estimated to be less than 5% for each telescope. For all the data reported in this paper, these errors were combined with the associated statistical errors.

III. MISSING CHARGE ΔZ

When one looks at an inclusive measurement for a nearly symmetric binary splitting of a light system such as $^{32}S+^{12}C\rightarrow^{44}Ti^*$, the presence of products with about one-half the mass of the compound nucleus does not prove the existence of a fission process. In particular, for a large enough incident energy one can even expect significant contributions from incomplete fusion evaporation residues[10] or incomplete deep inelastic collision fragments.[11] Also, no model independent distinction between symmetric and asymmetric decay modes is possible due to secondary evaporation. In order to avoid most of the above difficulties, the main emphasis in this work was on the coincidence measurements.

Figure 2 presents energy and angle integrated charge distributions for Z_1-Z_2 coincidences. The diagonal line given by $Z_1+Z_2=Z_P+Z_T=Z_{CN}=22$ corresponds to binary reactions with no charged particle evaporation. Here, Z_P, Z_T, Z_{CN}, Z_1, and Z_2 denote, respectively, the atomic numbers of the projectile, target, composite system, and of the detected fragments in the two telescopes. However, the main bulk of the events are spread around lines $Z_1+Z_2\simeq 20$ for nearly symmetric events, and $Z_1+Z_2\simeq 18$ for protectilelike and targetlike pairs. Thus the most probable missing charge Z was found to be 2–3, which is most likely lost through particle emission from the excited composite system and/or from any of the reaction partners. A somewhat smaller total charge loss for the nearly symmetric products than for more asymmetric splits was also noticed for the $^{12}C+^{40}Ca$ system.[1]

Recently, ^{32}S-induced reactions were studied on a number of targets between ^{16}O and ^{58}Ni.[12] The average amount of evaporated charge was found to increase linearly with c.m. energy. Such a feature can be expected for a fully relaxed phenomenon. Our missing Z value for nearly symmetric events agrees well with the above systematics, without complete exclusion of competition between fission and particle evaporation processes.[13]

IV. ANGULAR CORRELATIONS

In Figs. 3–5 are shown the in-plane laboratory angular correlations of different Z_1,Z_2 pairs measured with the two telescopes placed at equal angles but on opposite sides of the beam direction, $\theta_1=\theta_2$.

Figure 3 presents angular correlations between $Z_1=9$–11 and all residues $Z_2=5$–16 of the complementary fragments. This kind of presentation facilitates com-

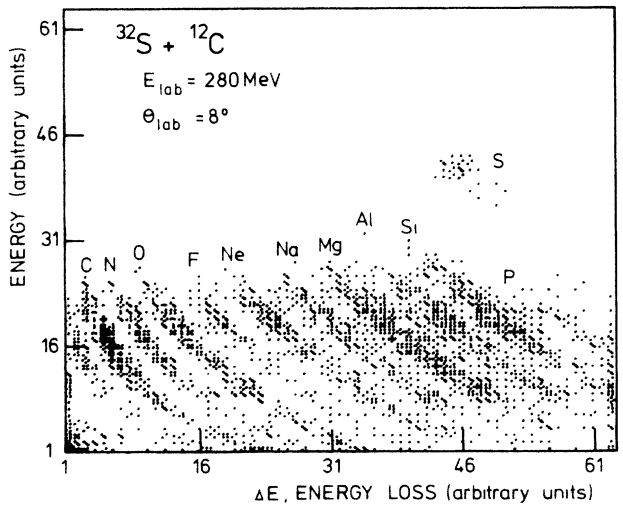

FIG. 1. E vs ΔE map for reaction products from the 280 MeV $^{32}S+^{12}C$ reaction

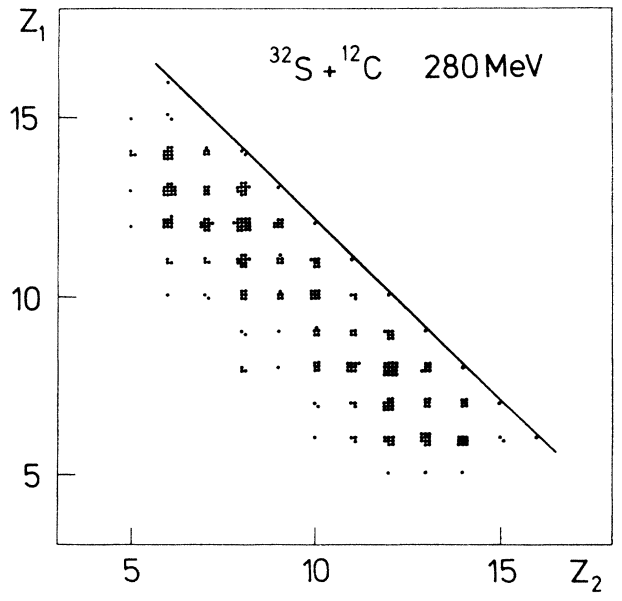

FIG. 2. Z_1-Z_2 correlation plot. The line corresponds to $Z_1+Z_2=Z_{CN}=22$.

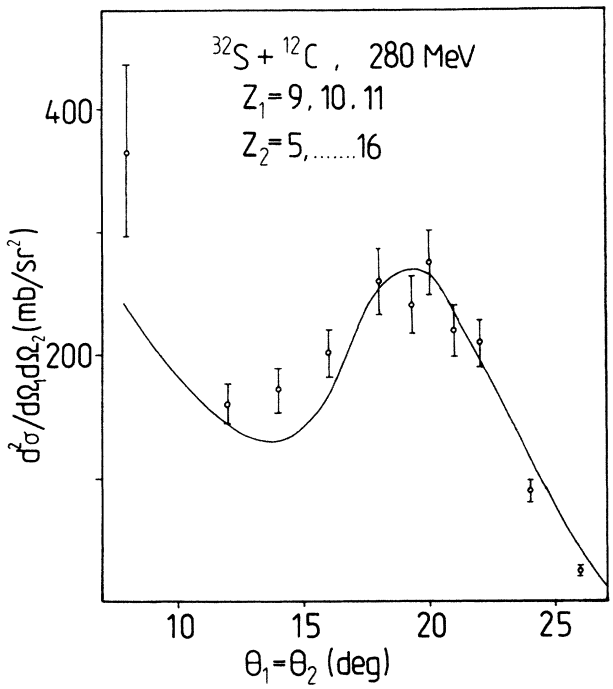

FIG. 3. In-plane angular correlation $\theta_1=\theta_2$ between $Z_1=9-11$ and all residues ($Z_2=5-16$) of the complementary fragments. The curve is Monte Carlo prediction for symmetric decay, TKE=32.5 MeV, $S_Q^2=25.8$ MeV^2, and $S_1^2=S_2^2=4.12\times10^{-5}c^2$ (see text).

parison between the inclusion and coincidence data (see Sec. V).

Figure 4 contains cases later classified as binary decay followed by light particle evaporation from fully accelerated fragments. Cases classified as evaporation or emission of light particles before binary splitting are displayed in Fig. 5. In the following paragraphs we will explain and justify such a classification.

One can argue that the postscission evaporation should contribute much more to the cross section than the prescission evaporation. This is based on the assumption that first chance evaporation or emission of light particles and corresponding loss of angular momentum should reduce considerably the probability of symmetric or almost symmetric splitting. Some experiments on ^{32}S induced reaction support this conjecture.[12] We therefore treat the data in the following analysis as if only postscission evaporation is present. It will also be shown that not all our data can be explained by this assumption.

Temporarily, we adopt in the following the postscission evaporation picture. We shall denote in this work all reaction parameters and cross sections before evaporation by primed symbols and after evaporation by unprimed ones.

The first row of data in Fig. 4 presents laboratory angular correlations for fragments pairs with $Z_1'=Z_1$ and $Z_2'=Z_2$ ($\Delta Z=0$). The case $Z_1'=11, Z_2'=11$ is classified as the symmetric decay; the $Z_1'=10, Z_2'=12$ and $Z_1'=9, Z_2'=13$ cases are classified as asymmetric decays.

The angular correlations are peaked at lab angles around 20°. For a binary process the main correlation angle $\theta_s=\theta_1=\theta_2$ is related to the TKE by

$$\tan^2\theta_s=\frac{4A_1'A_2'}{A_P(A_T+A_P)E_P}\mathrm{TKE}-\left[\frac{A_1'-A_2'}{A_P+A_T}\right]^2, \quad (1)$$

where A_P, A_T, A_1', and A_2' denote, respectively, the mass numbers of the projectile, target, and primary fragment nuclei. E_P is the lab incident energy and TKE is the total kinetic energy. In this work we assume $A_i'=2Z_i'$, where $i=1$ or 2.

Because the total kinetic energy release is very similar for symmetric and slightly asymmetric splittings of light systems (see Sec. VI), the mean correlation angle should decrease with increasing fragmentation asymmetry. Figure 6 shows the experimental $\theta_s(\Delta Z)$ dependence for all the correlation curves of Fig. 4. The θ_s values were extracted from the correlation data using a center of gravity

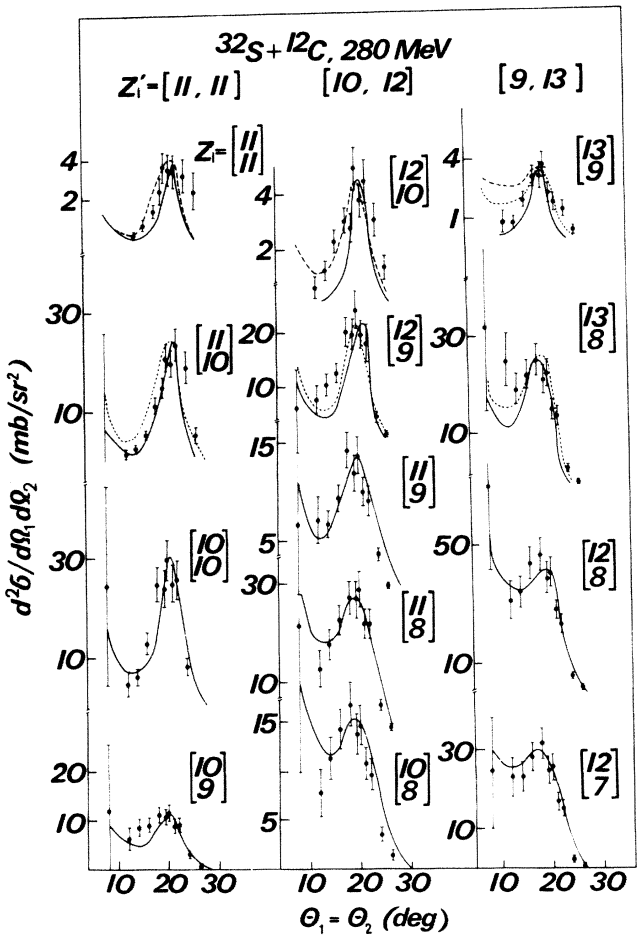

FIG. 4. In-plane angular correlation $\theta_1=\theta_2$ of cases classified as binary decay followed by evaporation of light particles from fully accelerated fragments. The curves are Monte Carlo calculations with parameters described in text (solid line, $A_i=2Z_i$; dotted line, emission of additional neutron from heavier fragment; dashed line, emission of additional neutrons from both fragments).

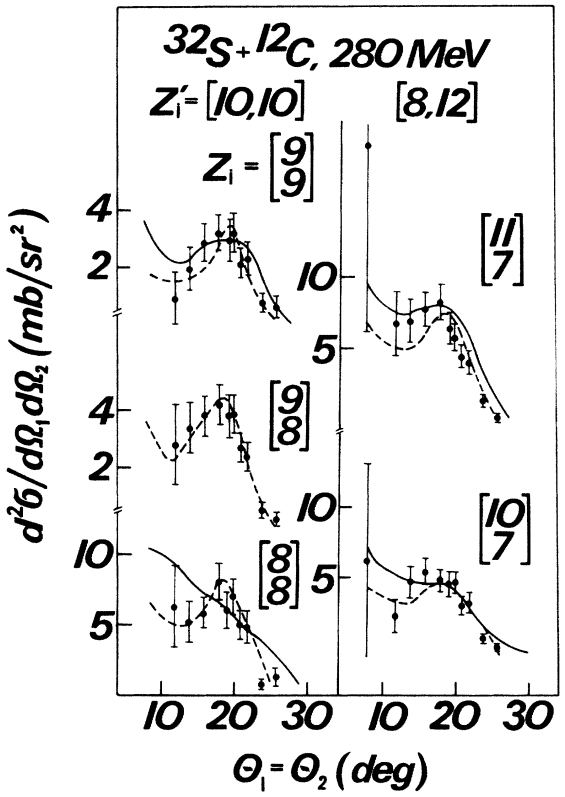

FIG. 5. In-plane angular correlation $\theta_1=\theta_2$ of cases classified as evaporation or emission of an α particle before binary splitting. The solid curves are the corresponding Monte Carlo calculations according to Fig. 7(a) kinematics. The dotted curves correspond to the prescission evaporation of an α particle [see Figs. 7(b) and 7(c)].

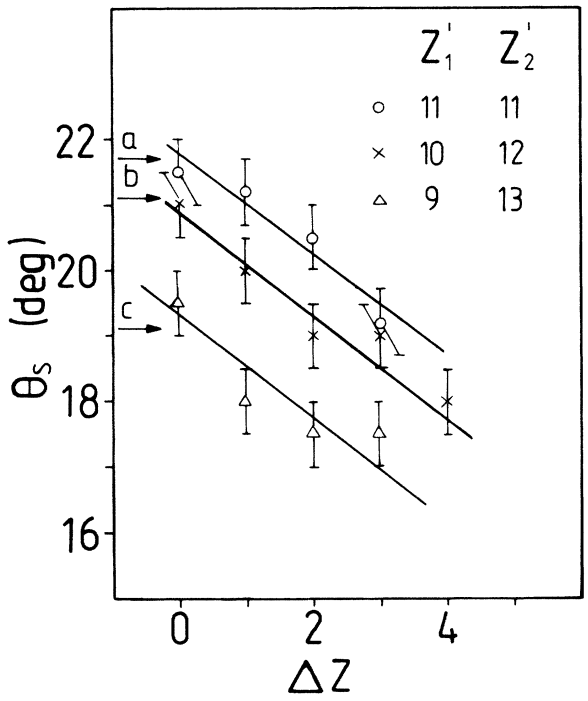

FIG. 6. Position of θ_s vs ΔZ dependence for correlation curves from Fig. 4. Arrows indicate the predictions of θ_s for an average value of TKE=32.3 MeV.

estimation. Inspection of Fig. 6 shows that the $\theta_s-\Delta Z$ points are grouped around three different lines labeled a, b, and c. For $\Delta Z=0$ corresponding to the data shown in the first row of Fig. 4, the θ_s dependence on the asymmetry of splitting agrees quite well with predictions of formula (1) within the uncertainties associated to the θ_s determining procedure. The average value of the TKE, 32.3 MeV, was extracted from $\Delta Z=0$ points. In Fig. 6 the corresponding values of θ_s are indicated by arrows. For each group of points, θ_s decreases with increasing ΔZ. It will be shown by Monte Carlo calculations that the $\theta_s(\Delta Z)$ dependence is a consequence of particle evaporation from primary decay fragments. Therefore, we classify all points corresponding to line a as the symmetric decay and all points corresponding to lines b and c as the asymmetric decays.

It should be remembered that evaporation of light particles is a statistical process. The total missing charge ΔZ is to be distributed among two fragments with quite a large variation. The final mass distribution must have larger variance due to neutron evaporation. Consequently, each correlation curve classified in Figs. 4 and 6 as belonging to definite primary asymmetry may have some admixture of other contributions. However, reasonably good separation of the points grouped around lines a, b, and c in Fig. 6 indicates that such contributions are not too significant. Another regularity seen in Fig. 4 is the broadening of the correlation curves with increasing ΔZ. Due to this broadening the tails of the two maxima always present in the correlation curves at $\theta_1=\theta_2=\theta_s$ and $\theta_1=\theta_2=0°$ contribute to an increase of the observed cross section in the angular region between 0° and θ_s for large ΔZ.

A. Monte Carlo calculations

In order to gain a quantitative understanding of the maxima shifts and the broadening of the correlation curves, Monte Carlo calculations have been performed. Application of this method enabled us to avoid difficulties in the lab to c.m. transformation which are expected for binary reactions of light systems in the presence of particle evaporation.[1]

The calculations were performed in velocity space [see Fig. 7(a)] where $\mathbf{V}_0$ is the velocity of the composite system, and $\mathbf{V}'_1$ and $\mathbf{V}'_2$ denote the initial c.m. velocities of fragments 1 and 2, respectively. $\mathbf{V}'_1$ and $\mathbf{V}'_2$ were calculated for a given TKE and a primary mass asymmetry. The Q-value fluctuations at the scission point given the distribution of the c.m. kinetic energies around the average value TKE. This distribution was approximated by a Gaussian function with a variance $S_Q^2=25.8\pm3.2$ MeV^2. This value of S_Q^2 was calculated from the rotating liquid drop model (see Sec. VI). In our calculations a random number generator gave the initial directions of the frag-

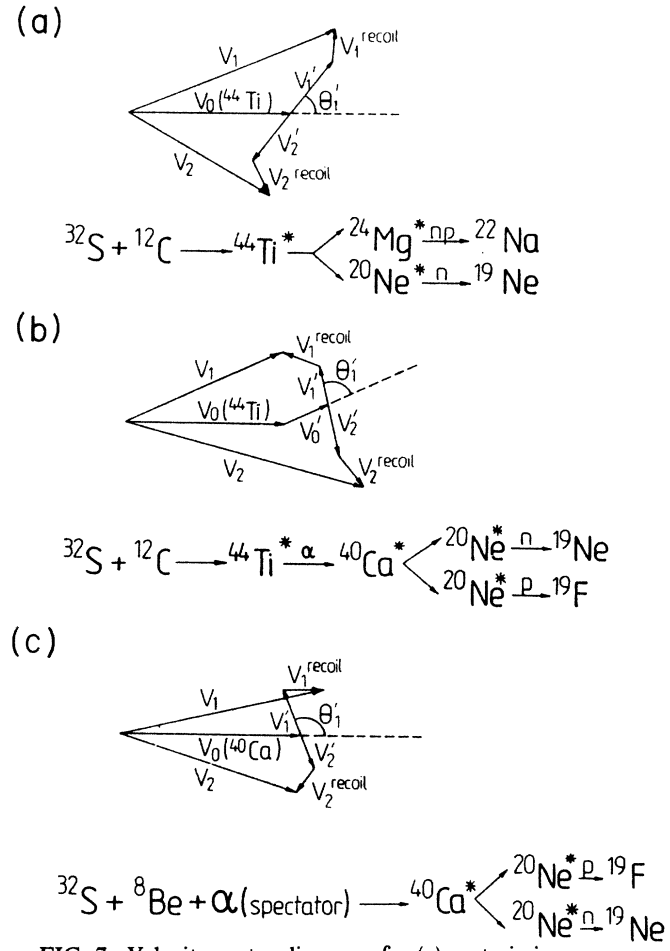

FIG. 7. Velocity vector diagrams for (a) postscission evaporation of light particles, (b) prescission evaporation of light particles, and (c) incomplete fusion followed by fission and finally evaporation from fragments.

ments according to an assumed c.m. angular distribution $d\sigma/d\Omega \sim 1/\sin\theta_1'$, where θ_1' is fragment 1 angle in the c.m. system. To determine the c.m. average recoil velocity v_i^{recoil}, $i=1$ or 2, for a given fragment, a Gaussian probability distribution was assumed for each Cartesian component with a corresponding variance S_i^2 (for more details, see Ref. 14). This variance should increase both with the increasing number of evaporated nucleons, ΔA, and the decreasing mass A_i' of the evaporating fragment (larger recoil). The dependence on ΔA may be understood in analogy to a random-walk problem, previously solved by Smoluchowski for Brownian motion.[15] In a random walk the average distance from the starting point is proportional to the square root of the number of steps. In our case consecutive steps correspond to the consecutive nucleon evaporations from the fragment.

Both dependences are combined in the formula derived by Lide:[16,17]

$$S_i^2 = K\frac{\Delta A_i}{(A_i'-\Delta A_i)^2}T_i \ , \tag{2}$$

where ΔA_i denotes the total mass evaporated by a given fragment with an initial mass A_i' and the nuclear temperature T_i defined by[17]

$$T_i = \left[\frac{E_i^*}{a}\right]^{1/2} , \tag{3}$$

where E_i^* is the excitation energy of the fragment assumed proportional to its mass A_i', and $a=(A_i'/8)$ MeV^{-1} is the level density parameter. Due to Q-value fluctuations at the scission point, TKE and, consequently, fragment excitation energies are given by separate distributions. The excitation energy distribution was replaced in our calculations by an average value E_i^*. The resulting additional broadening is represented in Eq. (2) by a phenomenological factor K. The angular distribution of recoil velocities v_i^{recoil} was assumed to be isotropic. As the intrinsic spin of each fragment can be assumed to be $\sim 2\hbar$, an eventual focusing in the reaction plane can be neglected (see Sec. VI). Values of S_i^2 deduced from Eq. (2) are in reasonable agreement with data obtained for fusion evaporation residues and with the Monte Carlo Hauser-Feshbach calculations.[14] The final velocity of a fragment in the lab system is given by

$$\mathbf{V}_i = \mathbf{V}_0 + \mathbf{V}_i' + \mathbf{V}_i^{\text{recoil}} \ . \tag{4}$$

This Monte Carlo model has three free parameters: the primary mass asymmetry A_1'/A_2', the total c.m. kinetic energy TKE and the parameter K. Asymmetry A_1'/A_2' was assigned for each case according to the classification given in Figs. 4 and 6. Values of the remaining two parameters, TKE$=35.1\pm1.5$ MeV and $K=2.2\pm0.4$, were obtained from fits to the correlation curve $Z_1=Z_2=10$ ($\Delta Z=2$), which has the largest cross section in the group of symmetric splittings.

The average temperature T_i of fragments was found to be 2.26, 2.66, and 2.30 MeV for corresponding primary mass asymmetries $\frac{22}{22}$, $\frac{20}{24}$, and $\frac{18}{26}$, respectively.

Angular correlations calculated from this model [Fig. 7(a) kinematics] are plotted by solid lines in Fig. 4. The overall good agreement may be observed. For some cases it can be improved by adding neutron evaporation, as indicated in some Fig. 4 cases by dotted and dashed lines. The neutron evaporation was included by modifying ΔA_i in formula (2).

Figure 8 shows contributions to $d^2\sigma/d\Omega_1 d\Omega_2$ from the detector angular acceptance (dotted curve), combined either with the Q-value fluctuation (dashed line) or the evaporation recoils effect (dotted-dashed line). The three combined effects are shown as a solid line. As one can see, these contributions not only broaden, but also shift the maxima of the angular correlation curves and even change their shapes.

Not all experimental angular correlations could be clearly classified in Fig. 4 according to the proposed systematics of Fig. 6. Figure 5 includes such cases with $\Delta Z=4$ and 5. Here solid lines represent Monte Carlo predictions following Fig. 7(a) kinematics. One can notice the large discrepancies with the data. As another kinematical assumption, we also studied the prescission emission of an α particle. In this case two different

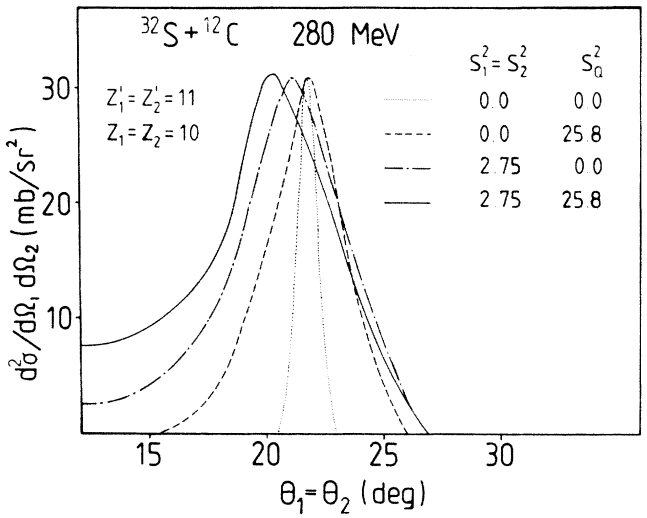

FIG. 8. Contributions from the detector angular acceptance, the Q-value fluctuation, and the evaporation recoils to the overall shape of the correlation curve. S_i^2 values are to be read in $10^{-5}c^2$ units. S_Q^2 is expressed in MeV^2 units.

mechanisms were proposed following Figs. 7(b) and 7(c). The first assumes prescission α particle evaporation from the compound system sequentially followed by a fission process and light particle evaporation from the nascent fragments. The second supposes the breakup of the ^{12}C target nucleus followed by an incomplete fusion mechanism, then fission and finally evaporation from fragments. Here the α particle from ^{12}C breakup is treated as a spectator. Both kinematic hypotheses (dotted line) gave similar and overall comparable agreement with the experimental data, at least better than the solid line.

It should be pointed out that in these Monte Carlo calculations a $1/\sin\theta_1'$ angular distribution shape was assumed for the primary fission fragments, which resulted in good agreement with the experimental data over a whole range of laboratory angles from 8° up to 30°. This roughly corresponds to a range of c.m. angles of 30°—170°.

B. Cross sections

In order to evaluate angle integrated cross sections of binary fragmentation processes, we have normalized the Monte Carlo predictions to experimental angular correlations of Figs. 4 and 5 according to the procedure described in Ref. 1. The results are listed in Tables I and II. They give partial cross sections for particular splitting pairs. Quoted errors reflect the experimental errors on data points (see Sec. II) and the statistical error of the Monte Carlo procedure.

In order to obtain cross sections for different modes of primary splitting of ^{44}Ti, we have summed up cross sections for particular pairs corresponding to symmetric and asymmetric modes, respectively. Figure 9 presents a charge spectrum of primary splitting. For symmetric splitting it displays the cross section value of column 4 of Table I and, for asymmetric cases, the corresponding values divided by 2 in order to avoid double counting. As seen from Table II, the contributions from the prescission mechanism are as small as expected.

V. ANGULAR DISTRIBUTIONS

Figure 10 shows the inclusive lab angular distributions for individual Z values between 7 and 13. Unfortunately, in this case the associated reaction partner(s) is (are) undefined; thus we are unable to evaluate effects such as the postscission or prescission evaporation or emission of light particles. Consequently, we are unable to assign angular distributions from Fig. 10 to particular fission modes as they were defined in Sec. IV. However, in order to check once more the consistency of our data analysis, we have compared cross sections from inclusive and coincidence data from the $Z = 9$, 10, 11 bins which completely cover the region of symmetric splitting and partially the region of asymmetric splitting ($Z_1' = 10$, $Z_2' = 12$). As

TABLE I. The cross sections for pair correlation and summed up cross sections corresponding to symmetric and asymmetric modes of decay of the postscission picture of the reaction.

(A_1',Z_1') pairs	(A_i,Z_i) pairs	$\sigma^{Z_1Z^2}_{A_1A_2}$ (mb)	$\sigma_{A_1'A_2'}$ (mb)
(22,11) (22,11)	(22,11) (22,11)	0.009±0.003	0.89±0.16
	(20,10) (22,11)	0.21 ±0.06	
	(20,10) (20,10)	0.39 ±0.12	
	(18,9) (20,10)	0.28 ±0.09	
(20,10) (24,12)	(20,10) (24,12)	0.012±0.005	2.35±0.40
	(18,9) (24,12)	0.31 ±0.09	
	(18,9) (22,11)	0.27 ±0.09	
	(16,8) (22,11)	0.86 ±0.26	
	(16,8) (20,10)	0.90 ±0.27	
(18,9) (26,13)	(18,9) (26,13)	0.007±0.002	2.30±0.49
	(16,8) (26,13)	0.21 ±0.06	
	(16,8) (24,12)	1.07 ±0.36	
	(14,7) (24,12)	1.01 ±0.33	

TABLE II. The cross sections for pair correlation corresponding to symmetric and asymmetric decay modes for the prescission picture of the reaction.

(A_i',Z_i') pairs	(A_i,Z_i) pairs	$\sigma_{A_1A_2}^{Z_1Z_2}$ (mb)
(20,10) (20,10)	(18,9) (18,9)	0.04±0.01
	(16,8) (18,9)	0.08±0.02
	(16,8) (16,8)	0.17±0.05
(16,8) (24,12)	(14,7) (22,11)	0.14±0.04
	(14,7) (20,10)	0.12±0.04

coincidences, we have taken here the bins between $Z_1=9-11$ and all the associated residues with charges Z_2 between 5 and 16 (Fig. 3). The corresponding inclusive angular distribution is shown in Fig. 11. The solid lines in Figs. 3 and 11 sketch the prediction of the Monte Carlo calculation, with TKE=32.5 MeV and $S_Q^2=25.8$ MeV^2, both values being the same as in Sec. IV. The variances of the recoil velocity distribution could not be calculated from Eq. (2) because for inclusive data the values of ΔA_i are unknown. The variances, treated here as free parameters, were found to be $S_1^2=S_2^2=4.12\times10^{-5}c^2$. For comparison, values of S_i^2 calculated from Eq. (2) for cases presented in Fig. 4 are $1\div15\times10^{-5}c^2$.

The overall shape is in fair agreement with the experimental results, except at small angles, where the inclusive data indicate some excess, probably resulting from other reaction mechanisms.

A normalization of Monte Carlo predictions to experimental data from Figs. 3 and 11 provides total cross sections of 6.1±1.3 and 9.4±1.1 mb, respectively.

VI. ROTATION LIQUID DROP MODEL CALCULATIONS

Results of this work for the $^{32}S+^{12}C$ binary decay reaction together with observations made for other light systems,[1] $46\leq A\leq52$, may be indicative of a fusion-fission–like mechanism conveniently described in terms of the rotating liquid drop model.

In the $^{32}S+^{12}C$ reaction the colliding system at 280 MeV incident energy becomes excited, very soon after contact, to energies over 70 MeV, where shell effects are expected to vanish. In the absence of such effects a liquid drop leptodermous expansion of the energy of a nucleus-like system is fairly well reproduced down to very small

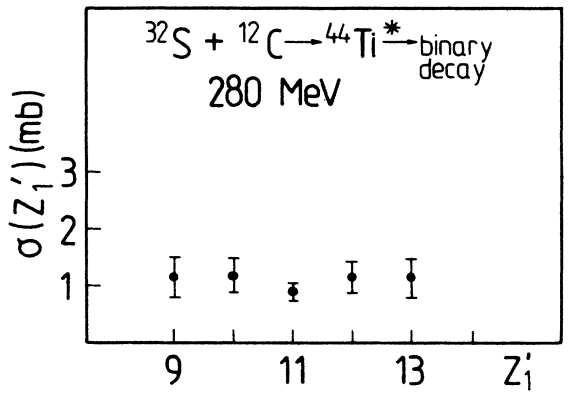

FIG. 9. Z spectrum of primary splitting process of ^{44}Ti.

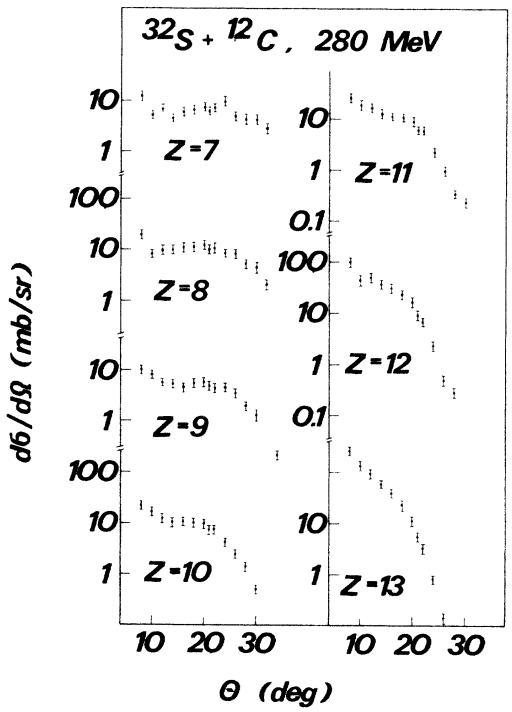

FIG. 10. Inclusive laboratory angular distributions for individual Z values.

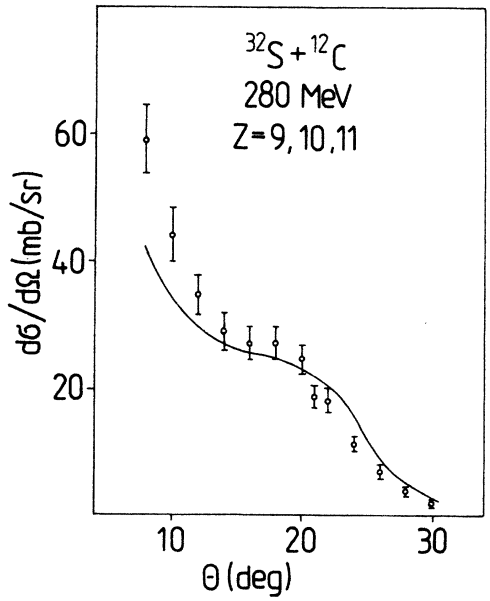

FIG. 11. Inclusive angular distribution for $Z=9$, 10, and 11 bins.

mass numbers (see, e.g., Ref. 18, Fig. 12 and Ref. 19, Fig. 25).

In our RLDM calculations we used the simple parametrization of nuclear shapes following Ref. 3, with distance variable

$$\rho=\frac{r}{R_1+R_2}\ ,$$

neck variable

$$\lambda=\frac{d_1+d_2}{R_1+R_2}\ , \tag{5}$$

and asymmetry variable

$$\Delta=\frac{R_1-R_2}{R_1+R_2}\ .$$

The R_1, R_2, d_1, d_2, and r parameters are defined according to Fig. 12. The nuclear shapes are assumed to be axially symmetric and correspond to two spheres modified by a smoothly fitted portion of a quadratic surface of revolution. Such simplified parameterization gives reasonable agreement with the liquid drop model of Cohen, Plasil, and Świątecki.[4,5]

Figure 13 shows locations in the (ρ,λ) plane $(\Delta=0)$ of some of the saddle points (crosses) together with some of the local minima of the RLDM potential (dots). Such minima may be interpreted as shapes of the compound system $^{32}S+^{12}C\rightarrow^{44}Ti$ for consecutive values of angular momentum L. The model predicts that there are no stable ^{44}Ti nuclei with angular momenta higher than $43\hbar$, in agreement with the calculations of Wilcke *et al.*[20] As seen from Fig. 13, saddle points of ^{44}Ti are located quite close to the scission line.

As an example, the bottom part of Fig. 14 represents a (ρ,λ) $(\Delta=0)$ map of the RLDM potential $E_{\rm pot}$ for $L=36\hbar$ in the vicinity of the saddle point. The position of the scission point is marked by a cross.

The RLDM energies of the nucleus at saddle and scission points determine the effective reaction Q value and the total kinetic energy of fission fragments. The TKE is given as

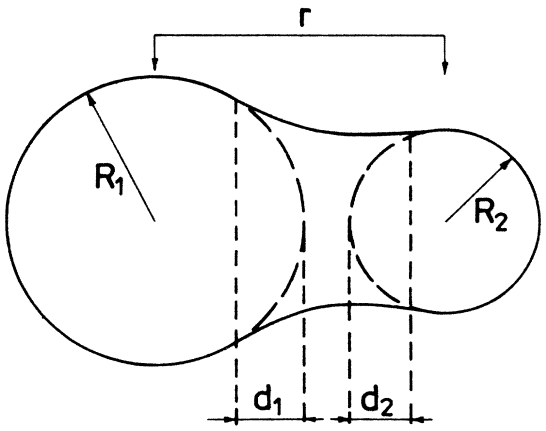

FIG. 12. Parametrization of the nuclear shapes.

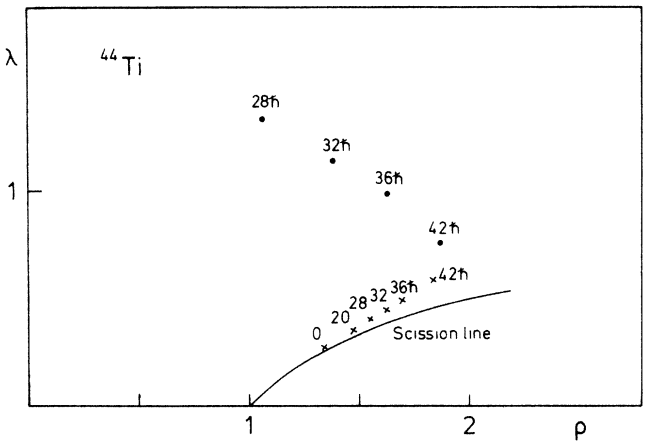

FIG. 13. Location in the (ρ,λ) plane of some of the states of the compound nucleus, ^{44}Ti (dots), together with some of the corresponding saddle points (crosses).

$$\mathrm{TKE}=E_C^{\rm sc}(\mathrm{int})+E_{\rm rot,rel}^{\rm sc}+E_{\rm kin}\ , \tag{6}$$

where $E_C^{\rm sc}(\mathrm{int})$ is the Coulomb interaction energy of fragments at scission point, and $E_{\rm rot,rel}^{\rm sc}$ is the rotation energy

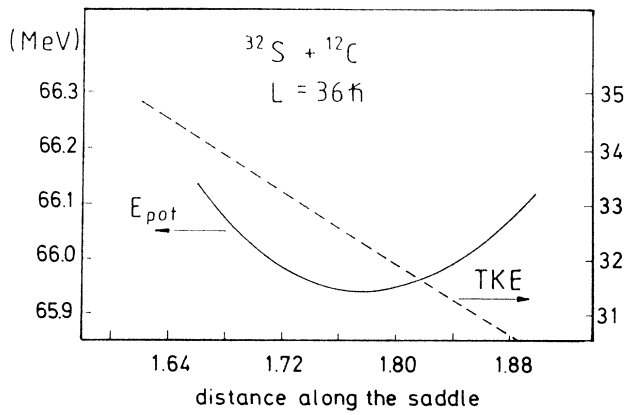

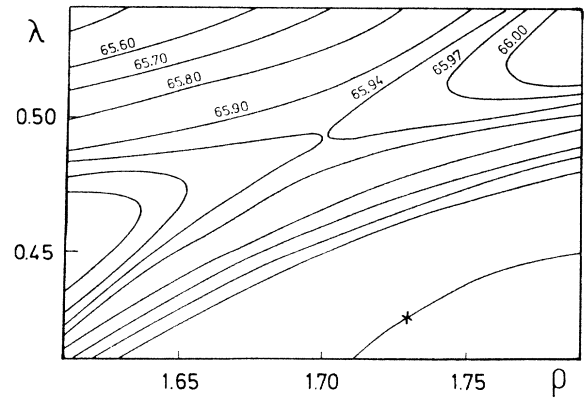

FIG. 14. Map of the RLDM potential, $E_{\rm pot}$, in the (ρ,λ) plane $(\Delta=0)$ for $L=36\hbar$ in the vicinity of the saddle point (bottom part). Behavior of $E_{\rm pot}$ (solid line) and of corresponding TKE (dashed line) as a function of the distance along the saddle.

of the relative motion at scission. The translation kinetic energy gained by the system between saddle and scission points is denoted $E_{\rm kin}$. The $E_C^{\rm sc}({\rm int})$ is given by numerical integration, while $E_{\rm rot,rel}^{\rm sc}+E_{\rm kin}$ may be obtained by the total energy conservation of the system between saddle and scission points. Finally, one obtains

$$\begin{aligned}{\rm TKE}=&E_C^{\rm sc}({\rm int})+E_{\rm rot,rel}^{\rm sa}+E_s^{\rm sa}-E_s^{\rm sc}\\&+E_C^{\rm sa}-E_C^{\rm sc}+E_{\rm rot,1}^{\rm sa}-E_{\rm rot,1}^{\rm sc}\\&+E_{\rm rot,2}^{\rm sa}-E_{\rm rot,2}^{\rm sc}-E_{\rm diss}\ .\end{aligned}\tag{7}$$

Here, $E_s^{\rm sa}$, $E_s^{\rm sc}$, $E_C^{\rm sa}$, $E_C^{\rm sc}$, $E_{{\rm rot},i}^{\rm sa}$, and $E_{{\rm rot},i}^{\rm sc}$ are, respectively, the surface, Coulomb, and fragment intrinsic rotation energies at saddle and scission points; $E_{\rm rot,rel}^{\rm sa}$ and $E_{\rm diss}$ denote the saddle relative rotational energy and the dissipated energy of the system in its motion from the saddle to the scission point.

The TKE may be calculated from Eq. (7) with different degrees of accuracy. The surface, Coulomb, and fragment intrinsic rotation energies at scission and saddle points are very similar and $E_{\rm diss}$ is nearly zero since the distance between these two points is small, as stated earlier. Consequently, in a first approximation,

$${\rm TKE}\simeq E_C^{\rm sc}({\rm int})+E_{\rm rot,rel}^{\rm sa}\ .\tag{8}$$

All but the last component of Eq. (7) can be obtained from the rotating liquid drop model. In order to calculate $E_{\rm diss}$, one has to solve a dynamical equation of motion with a proper energy dissipation function. One possible approach is presented in Ref. 3. For $L=36\hbar$, $E_{\rm diss}=0.7$ MeV.

In Fig. 15 the fragment total c.m. kinetic energy from ^{44}Ti symmetric fission predicted by Eqs. (7) (solid line) and (8) (dashed line) is presented as a function of the total angular momentum L. Since the saddle-to-scission energies are negligible here [see Eq. (8)], the TKE is mainly the sum of the Coulomb, $E_C^{\rm sc}({\rm int})$, and relative rotational motion, $E_{\rm rot,rel}^{\rm sa}$, energies, which are also shown. The hatched band in Fig. 15 represents the measured TKE$=32.5\pm1.5$ MeV. The liquid drop total kinetic energy curves increase with L and cross the experimental band, suggesting an angular momentum window for fission from $33\hbar$ to $38\hbar$. Within this window the Coulomb and rotation components of the total kinetic energy are of equal importance.

It is worth mentioning that within this window most of the angular momentum is carried by the orbital motion of the fragments and only 12% is contained in spins of the two fission fragments. This value comes both from the RLDM (Ref. 3) and dynamical calculations (Ref. 4) and is supported by γ multiplicity measurements.[21]

The total kinetic energy depends very little on the initial asymmetry. For $A_1'/A_2'=\frac{22}{22}$ and $\frac{18}{26}$ the difference in TKE is smaller than 0.2%.

The RLDM provides not only the mean value but also the distribution of the TKE. In the fission process the excitation energy of a system goes into collective degrees of freedom, inducing, finally, an increased deformation at the saddle point. The upper part of Fig. 14 shows a nearly parabolic behavior of $E_{\rm pot}$ as a function of the distance

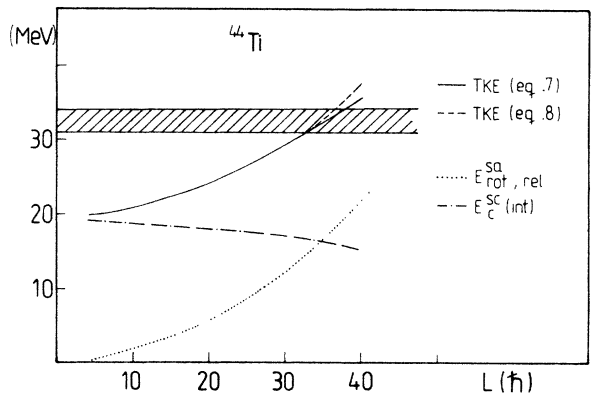

FIG. 15. The total kinetic energy of the fission fragments from ^{44}Ti predicted by Eqs. (7) (solid line) and (8) (dashed line) vs total angular momentum. The hatched band represents the measured TKE. The separate contributions for the Coulomb and rotational energies are also given.

along the saddle (solid line). Fission occurs not only at the minimum of $E_{\rm pot}$ but also in its neighborhood due to the nuclear temperature T at the saddle. This causes fluctuations of the fission Q value and results in a distribution of TKE. As seen in Fig. 14, a relatively small fluctuation of $E_{\rm pot}$ results in a much larger fluctuation of the corresponding TKE, the latter being the sum of the Coulomb and rotation contributions (dotted straight line).[22,23] According to Ref. 23, the variance of the TKE distribution may be written as

$$\sigma_Q^2=\tfrac{1}{2}pT\ ,\tag{9}$$

where $p=c^2/k$ is an amplification factor. Here, k is the curvature of the parabola (solid curve) and c is the slope of the straight line (dashed line). The value of σ_Q^2 estimated this way for $L=36\hbar$ is equal to 25.8 ± 3.2 MeV^2. Within the angular momentum window it varies between 23.1 and 27.2 MeV^2 (see Fig. 15).

It was shown[23] that the shape of the mass distribution is related to the $E_{\rm pot}$ dependence on asymmetry at the saddle point. Figure 16 presents shapes of the potential energy of the ^{44}Ti compound nucleus as a function of Δ for consecutive values of L. For $L>30\hbar$ a minimum in the potential energy is seen for $\Delta=0$ and, as a consequence, one can expect a maximum yield at $\Delta=0$ for such partial waves. On the other hand, a maximum in the potential energy is present at $\Delta=0$ for $L<30\hbar$ and, consequently, such partial waves should exhibit a minimum yield for $\Delta=0$. It is reasonable to believe that a flat mass distribution should be a consequence of a flat potential energy curve versus Δ. This is in complete agreement with the experimental Z distribution measured in this work and displayed in Fig. 9. As seen from Fig. 16, this $L=30\hbar$ angular momentum is close to the values of the angular momentum window found from comparison with the TKE.

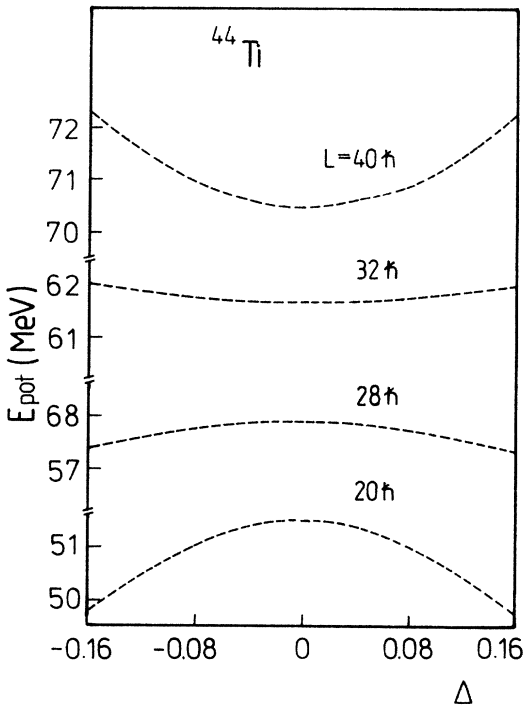

FIG. 16. Shapes of the potential energy of the ^{44}Ti compound nucleus as a function of Δ for consecutive values of L.

VII. SUMMARY AND CONCLUSION

The coincidence measurement presented and discussed in this study clearly established the symmetric and nearly asymmetric binary fragmentation of the ^{44}Ti nucleus formed in the $^{32}S+^{12}C$ reaction at 280 MeV incident energy.

A Monte Carlo procedure has been applied to describe the reaction mechanism in the presence of high excitation and secondary evaporation. It successfully described the fragment, Z, angular correlations assuming a symmetric or slightly asymmetric splitting, $1/\sin\theta'_1$ c.m. angular distribution, and a postscission or prescission emission of light particles. Both recoil effects and Q-value fluctuations were treated in detail.

It was found that the dominant reaction mechanism is the postscission evaporation, in agreement with previous results obtained for similar light systems.[1]

The most probable total c.m. kinetic energy TKE$=32.5\pm1.5$ MeV of decay fragments measured in this work provides a new value for the standard fission systematics. The first Viola paper[7] provides, for our case, the value of 36.9 MeV, but the recent value of Viola *et al.*[8] is 23.6 MeV.

Comparison between the experimental value of TKE and the RLDM prediction locates the angular momentum window for symmetric splitting between $33\hbar$ and $38\hbar$. This is very close to the value of $30\hbar$ at which the RLDM potential energy curve shows a flat dependence on the mass asymmetry, in agreement with the flatness of the experimental element distribution.

The RLDM predicts that most of the initial angular momentum in this reaction is converted to the orbital motion of the nascent fragments. Consequently, the rotation energy contributes about 50% to the total kinetic energy (TKE) of the fragments. This may explain the discrepancy observed between the experimental TKE value and the prediction of the Viola systematics.

However, it should be stressed that all the quantitative conclusions of our calculations are likely to be affected to some extent by refinements of the RLDM. These refinements may include, in addition to the shell effects which seem to be unimportant at such an excitation energy, both the finite nuclear interaction and the temperature dependence of the liquid drop model parameters.

Estimation of nuclear temperature effects is complicated and only few developments were achieved in this field. For example, in Ref. 24 a temperature of 3 MeV is estimated to lower the fission barrier of a compound nucleus by about 10%.

We tested the influence of the finite nuclear interaction at the saddle and scission points with the modified RLDM by Krappe *et al.*[25] This effect shifts the angular momentum window down by $3\hbar$.

It should be pointed out that our data can also be interpreted as statistical emission of intermediate-mass fragments from an excited composite system. Such a mechanism has been recently proposed by Sobotka *et al.*[26] for the reaction 90 MeV $^{3}He+^{nat}Ag$. However, it has been suggested that the statistical emission of intermediate-mass fragments, as well as the fission along the mass asymmetry coordinate, can be treated in an equivalent way.[23,27]

ACKNOWLEDGMENTS

The authors are indebted to Dr. A. J. Cole and Dr. Z. Sosin for fruitful discussions. Special thanks are due the Louvain-la-Neuve Cyclotron operating crew for providing an excellent beam. One of the authors (K.G.) wishes to acknowledge the warm hospitality of his colleagues at Kernforschungszentrum, Karlsruhe.

*Permanent address: Institute of Physics, Jagellonian University, and Institute of Nuclear Physics, Kraków, Poland.

[1]K. Grotowski, Z. Majka, R. Płaneta, M. Szczodrak, Y. Chan, G. Guarino, L. G. Moretto, D. J. Morrissey, L. G. Sobotka, R. G. Stokstad, I. Tserruya, S. Wald, and G. J. Wozniak, Phys. Rev. C **30**, 1214 (1984).

[2]See, e.g., M. Lefort, *Heavy Ion Collisions*, edited by R. Bock (North-Holland, Amsterdam, 1980), Vol. 2.

[3]J. Błocki and W. J. Świątecki, Lawrence Berkeley Laboratory Report No. LBL-12811, 1982 (unpublished).

[4]J. Blocki, K. Grotowski, R. Planeta, and W. J. Świątecki, Nucl. Phys. **A445**, 367 (1985).

[5]S. Cohen, F. Plasil, and W. J. Świątecki, Ann. Phys. (N.Y.) **82**, 557 (1974).

[6]T. Bengtsson, M. Faber, M. Płoszajczak, I. Ragnarsson, and S. Aberg, Lund Report No. 21, 1983 (unpublished).

[7]V. E. Viola, Jr., Nucl. Data Tables A **1**, 391 (1966).

[8]V. E. Viola, Jr., K. Kwiatkowski, and M. Walker, Phys. Rev. C. **31**, 1530 (1985).

[9]Ph. Deschepper, P. Lebrum, J. Lehmann, L. Palffy, and P. Pellegrin, Nucl. Instrum. Methods. **166**, 531 (1970); H. D. Betz, G. Hortig, E. Leischner, Ch. Schmelzer, B. Stadler, and J. Weihrauch, Phys. Lett. **22**, 643 (1966).

[10]H. Morgenstern, W. Bohne, W. Galster, K. Grabisch, and A. Kyanowski, Phys. Rev. Lett. **52**, 1104 (1984).

[11]A. Budzanowski, M. Bürgel, H. Fuchs, H. Homeyer, G. Ingold, U. Jahnke, G. Thoma, and J. Uckert, Verh. Dtsch. Phys. Ges. VI **20**, 375 (1985); F. Guzman Martinez and R. Reif, Nucl. Phys. **A436**, 294 (1985).

[12]J. Betz, H. Graef, R. Novotny, D. Pelte, and U. Winkler, Nucl. Phys. **A408**, 150 (1983).

[13]P. Grange and H. Weidenmüller, Phys. Lett. **96B**, 26 (1980).

[14]J. Gomez del Campo, R. G. Stokstad, J. A. Biggerstaff, R. A. Dayras, A. H. Snell, and P. H. Stelson, Phys. Rev. C **19**, 2170 (1979).

[15]M. Smoluchowski, Ann. Phys. (Leipzig) **21**, 756 (1906).

[16]R. W. Lide, Oak Ridge National Laboratory Report No. 3358, 1967 (unpublished).

[17]D. Hilscher, J. R. Birkelund, A. D. Hoover, W. U. Schröder, W. W. Wilcke, J. R. Huizenga, A. C. Mignerey, K. L. Wolf, H. F. Breuer, and V. E. Viola, Jr., Phys. Rev. C **20**, 576 (1979).

[18]W. D. Myers, and W. J. Świątecki, Nucl. Phys. **81**, 1 (1966).

[19]W. D. Myers, and W. J. Świątecki, Ann. Phys. (N.Y.) **55**, 396 (1969).

[20]W. W. Wilcke, J. R. Birkelund, H. J. Wollerskeim, A. D. Hoover, J. R. Huizenga, W. V. Schröder, and L. E. Tubbs, At. Data Nucl. Data Tables **25**, 389 (1980).

[21]K. A. Geoffroy, J. B. Natowitz, R. C. Eggers, and M. N. Namboodiri, Nucl. Phys. **A302**, 310 (1978); K. A. Geoffroy, J. B. Natowitz, R. C. Eggers, P. Kasiraj, and M. N. Namboodiri, *ibid.* **A302**, 333 (1978).

[22]W. J. Świątecki (unpublished); J. R. Nix, in *Proceedings of the Third Conference on Reactions Between Complex Nuclei,* edited by A. Ghiorso, R. M. Diamond, and H. E. Conzett (University of California Press, Berkeley, 1963).

[23]L. G. Moretto, Nucl. Phys. **A247**, 211 (1975).

[24]E. Tomasi, X. S. Chan, S. Leroy, C. Ngô, M. Barranco, Y. Vinas, and H. Ngô, Nucl. Phys. **A389**, 69 (1982).

[25]H. J. Krappe, J. R. Nix, and A. J. Sierk, Phys. Rev. C **20**, 992 (1979).

[26]L. G. Sobotka, M. A. Padgett, G. J. Wozniak, G. Guarino, A. J. Pacheco, L. G. Moretto, Y. Chan, R. G. Stokstad, I. Tserruya, and S. Wald, Phys. Rev. Lett. **51**, 2187 (1983).

[27]W. J. Świątecki, Austr. J. Phys. **36**, 641 (1983).